RESEARCH

Structural and electrical properties of cross-linked blends of Xanthan gum and polyvinylpyrrolidone-based solid polymer electrolyte

P. Saranya[1] · D. Vanitha[2] · K. Sundaramahalingam[3] · M. Nandhinilakshmi[1] · Shameem Abdul Samad[4]

Abstract

Research based on solid polymer electrolytes (SPEs) has been improved extensively over the past few decades owing to their abundance in nature, non-toxicity, low cost, and biodegradability. In this study, natural microbial polymer Xanthan gum (XG) and biodegradable synthetic polymer polyvinylpyrrolidone (PVP)-based SPEs are synthesized by the solution casting method. The improvement in the amorphous nature of the blend electrolytes is investigated using X-ray diffraction (XRD). The complex nature of the blended electrolytes is analyzed using Fourier Transform Infrared Spectroscopy (FTIR). The conductivity of the 2 XG/98PVP polymer complex is found to be maximum, with a value of 1.01×10^{-6} Scm^{-1} at room temperature observed by electrical impedance spectroscopy (EIS). Using a temperature-dependent plot, activation energy (E_a) is found to be minimum with a value of 0.21 eV for the higher conducting sample. From the Argand plot, the non-Debye nature of the polymer electrolytes is confirmed. The lowest relaxation time (τ) of 6.2×10^{-5} s is observed for the 2 XG/98PVP electrolyte by using the loss tangent spectra. Transference number analysis (TNA) is observed for the confirmation of conductivity due to ions by Wagner's polarization method.

Keywords Xanthan gum · PVP · XRD · FTIR · AC impedance · Activation energy

Introduction

Energy production, storage, and distribution are the critical requirements for companies and society in general. Low-cost solid-state batteries are essential in electronic industries for the growing equipment such as sensors, lightweight electrochemical devices [1–3]. In many electrochemical devices, electrolytes play an important role. The most popular electrolytes used in electrochemical devices are liquids, but they can pollute or harm the environment since they are difficult to handle during device construction and are prone to leak when the device is damaged. So, for device applications, solid or gel electrolytes are preferred. The solid polymer electrolytes (SPEs), which have several benefits including non-leakage, volumetric stability, and solvent-free conditions, are well recognized to be quite alluring. Additionally, they offer high mechanical and adhesive qualities to a variety of substrates, a broad electrochemical stability window, and ease of synthesis in many forms. The extensive use of synthetic polymer as an electrolyte in materials endangers ecosystems [4–6]. As a result, biodegradable polymers are needed for electrical applications because of its environmental friendliness [7]. Biopolymers are naturally found in living organisms and are naturally decomposed and reabsorbed. Biopolymers are superior alternatives to synthetic polymers because they are cheaper, environmentally benign, and have specialized functional groups that require little alteration to change their characteristics [8]. Biopolymers such as starch [9], cellulose [10], agar–agar [11, 12], pectin [13], alginate [14], carrageenan [15], chitosan [16], and natural gums [17] are generally used in the preparation of solid polymer electrolytes. The major

✉ D. Vanitha
vanibala2003@gmail.com

1 Multi-Functional Materials Laboratory, International Research Centre, Kalasalingam Academy of Research and Education, Krishnankoil 626 126, Tamil Nadu, India

2 Department of Physics, Kalasalingam Academy of Research and Education, Krishnankoil 626 126, Tamil Nadu, India

3 Department of Physics, Arulmigu Kalasalingam College of Arts and Science, Krishnankoil 626 126, Tamil Nadu, India

4 Department of Science and Humanities, Karpagam Academy of Higher Education, Coimbatore 641021, Tamil Nadu, India

drawback of individual bio-polymer electrolyte is low conductivity. Biopolymer based SPE consists mostly of a salt dissolved in a polymer matrix that results in an ionically conducting solid solution. However, the addition of salts can also increase the crystalline phase in SPE, which is not desirable because in such systems the amorphous phase is mainly responsible for high ionic conduction. The blending of polymers is the most optimistic and significant method that is generally used for synthesizing SPEs [18–24].

In recent years, many researchers focused on biopolymer-based environmentally friendly SPEs membranes to be used in electrochemical devices. Now a day, Gum based polymers are widely used in energy applications. Gums derived from plants, animals, and microorganisms are also polysaccharides. The majority of readily accessible gums have a propensity to gel when water is added; therefore, they have found use in the oil drilling, pharmaceutical, culinary, and cosmetic sectors.

Xanthomonas campestris is a plant-pathogenic bacterium (Gram-negative bacterium) that produces Xanthan gum (XG),a complex exo-polysaccharide [25]. XG is a natural anionic antioxidant biopolymer with a high molecular weight and high viscosity and is widely utilized in various industries, including the petrochemical, biomedical, and cosmetics sectors [26]. In the previous work, XG is used as a gel polymer electrolyte in many energy storage device applications such as supercapacitor and batteries [27–29]. The preparation of XG as a solid polymer electrolyte is quite difficult because of its superior rheological properties, such as the highly viscous nature of XG [30]. To prepare Xanthan-based solid polymer electrolytes, blending of two polymers is preferred. For environmental concern, a biodegradable polymer polyvinylpyrrolidone (PVP) is chosen for blending. PVP has good absorbency, film forming capacity, water solubility, biocompatibility, and less electrical conductivity, easily blends with biopolymers, and has rich physics in the charge transport mechanism [31, 32]. Besides that, plasticizers are usually added to enhance the amorphous phase of polymer matrix and, consequently, the ionic conductivity of the electrolyte.

Izabel Caldeira et al. [33] prepared the XG/Polyvinyl alcohol/ acetic acid based polymer electrolytes by varying the concentration of acetic acid. The acetic acid acts as the principal source of protons to obtain the good conductivity. G. S. Guru et al., (2010) reported blending of Xanthan gum with Poly (vinyl pyrrolidone) at different temperatures in 0.1 M NaCl solution. The semi-compatible nature of the blend was discussed [34]. Research articles related with the XG based SPEs in energy storage applications are very rare.

In this work, a new trial has attempted to blend the XG and PVP by using ethylene glycol (EG) as a cross-linker to improve the mechanical and thermal stability and the conductivity of the polymer electrolyte [35–37].

Materials

The biopolymer XG ($C_{35}H_{49}O_{29}$: monomer) with molecular weight 933.74 g/mol was purchased from Otto Chemie, PVP (K90) LR grade (monomer: C_6H_9NO molecular weight—111.142 g/mol) was bought from Sd Fine Chem. Ltd. (SDFCL) and EG ($C_2H_6O_2$) with 99% purity (GC) and molecular weight of 62.07 g/mol was procured from Merck Specialities Private Limited.

Preparation method

XG is represented by its high rheological and viscous properties. The molecular weight of XG is much higher than PVP. For the preparation of SPEs, XG can be taken at a small amount compared with PVP. XG and PVP are water-soluble. Polymer electrolytes were prepared using a simple solution-casting method. XG and PVP were taken as 0.5 wt.% XG/99.5 wt.% PVP, 1 wt.% XG/99 wt.% PVP, 1.5 wt.% XG/98.5 wt.% PVP, 2 wt.% XG/98 wt.% PVP, and 2.5 wt.% XG/97.5 wt.% PVP, and 0.65 ml of crosslinker EG was mixed with the blend. For the synthesis of the polymer matrix, a total of 1 g of blend polymers was taken. XG was dissolved in 40 ml of distilled water at 80 °C for 4 h by vigorous stirring. PVP was dissolved in 30 ml of distilled water at room temperature for 1 h. After the complete dissolution, the two polymers were mixed and stirred. Consequently, EG was added drop by drop with the compound solution. A homogenous solution was obtained after 24 h of steady stirring at 50 °C. The prepared solution was poured into Petri dishes with 7.2-cm diameter and placed in an oven at 50 °C for 24 h. The prepared films were peeled from the Petri dishes and kept in desiccators for further studies. Table 1 gives the notation for the prepared polymer electrolytes. The schematic illustration of preparation is shown in Fig. 1.

Table 1 Composition of polymer and their labels

Composition of polymers	XG (g)	PVP (g)	Notations
0.5 wt.% XG/99.5 wt.% PVP	0.04050	0.95949	0.5 XG/99.5 PVP
1 wt.% XG/99 wt.% PVP	0.07820	0.92177	1 XG/99 PVP
1.5 wt.% XG/98.5 wt.% PVP	0.11342	0.88657	1.5 XG/98.5 PVP
2 wt.% XG/98 wt.% PVP	0.14636	0.85363	2 XG/98 PVP
2.5 wt.% XG/97.5 wt.% PVP	0.17724	0.82275	2.5 XG/97.5 PVP

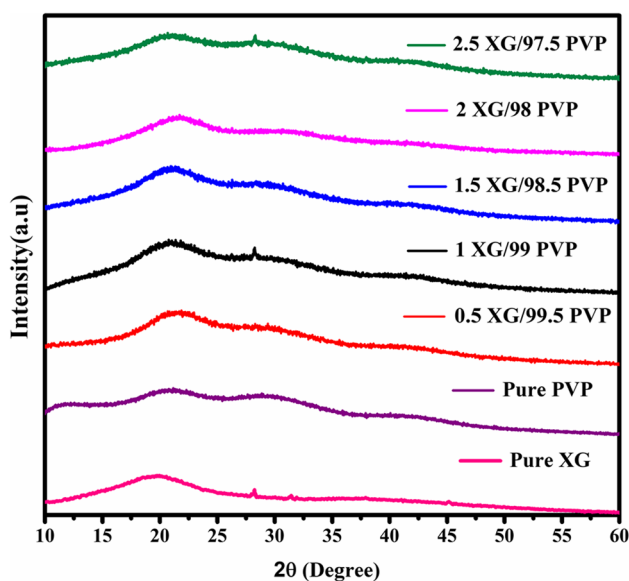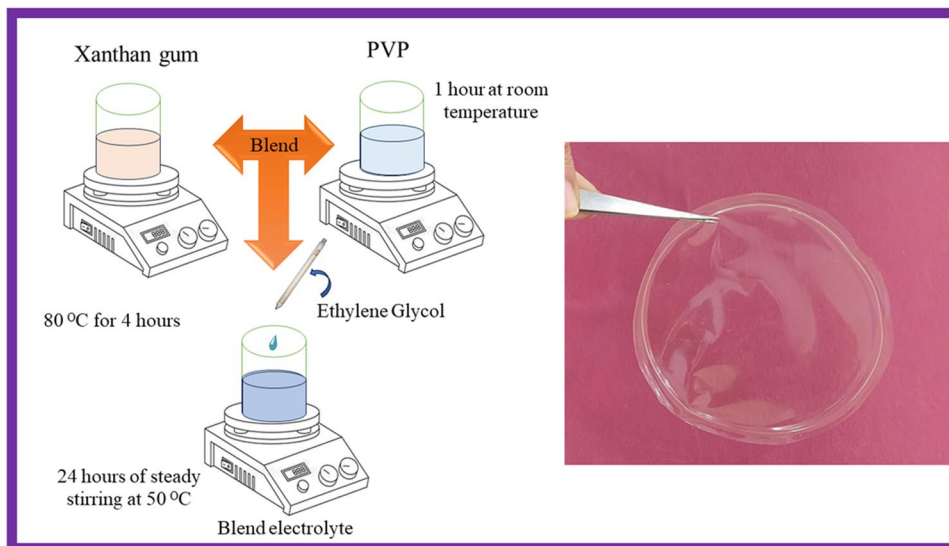**Fig. 1** Schematic illustration of the experimental method

Fig. 2 XRD pattern of prepared blend electrolytes

Table 2 FTIR band assignments of Pure XG, Pure PVP, Pure EG, and prepared blend electrolytes

Assignment	Wave number (cm^{-1})			
	Pure Xanthan gum	Pure PVP	Pure ethylene glycol	XG/PVP/EG blend electrolytes
O–H stretching	3308	3393	3294	3363
C–H stretching	2917	2951	2938	2942
C=O stretching	1607	1638	-	1645
C–H bending	1405	1437	1478	1435
C–N stretching	-	1292	-	1286
C–O stretching	1025	-	1036	1039

Result and discussion

X-ray diffraction analysis

XRD diffraction patterns of all the prepared polymer electrolytes are shown in Fig. 2. Pure XG has a semicrystalline structure and shows a noticeable hump at $2\theta = 20°$ and a small peak at $2\theta = 28.2°$, $31.4°$, and $45.1°$ [37]. PVP is an amorphous polymer and has a hump at $2\theta = 21.1°$, $29.1°$, and $40.4°$ [38]. By increasing the concentration of XG, the intensity of the hump decreases for all t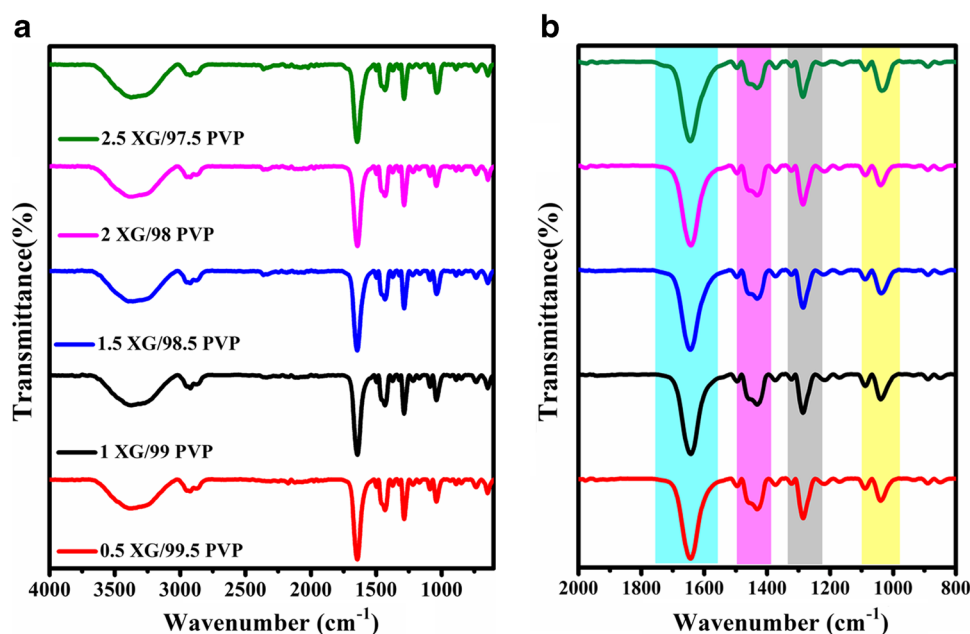he blend electrolytes. While increasing the concentration of XG, there exhibits a small peak at $2\theta = 28.2°$ for 1 XG/99 PVP. By increasing the concentration of XG, the peak is disappeared and reappears for 2.5 XG/97.5 PVP. The intensity of the hump is reduced for the samples 1.5 XG/98.5 PVP and 2 XG/98 PVP and there are no peaks corresponding to XG. This confirms the more amorphous nature of blended polymers. The variations in polymer wt.% affect the ordered arrangement inside the polymer membrane and reduce the semicrystalline nature of SPEs.

FTIR analysis

FTIR is an important analysis used to know about the interactions between the polymers. The wave numbers and their corresponding assignments for the prepared electrolytes are given in Table 2. Pure XG shows peaks at 3308 cm^{-1}, 2917 cm^{-1}, 1720 cm^{-1}, 1607 cm^{-1}, 1405 cm^{-1}, and 1025 cm^{-1}, which represent the OH, CH$_3$, and CH$_2$ functional groups, C=O stretching and bending vibrations

respectively [39]. The FTIR spectrum of PVP is observed in the region 3393 cm^{-1}(O–H groups), 2951 cm^{-1} (C–H), 1638 cm^{-1} (C = O), 1437 cm^{-1}(C = O stretching), and 1292 cm^{-1} (C–N stretching) [40]. The FTIR spectrum of EG shows transmittance peaks at 3294 cm^{-1} (vibration of the O–H group), 2938 cm^{-1} and 2875 cm^{-1} (C–H stretching), 1478 cm^{-1} (C = O stretching), and 1084 cm^{-1} and 1036 cm^{-1} (C − O stretching) [41, 42]. The FTIR spectrum of the XG/PVP/EG–blended polymer electrolytes is shown in Fig. 3a. The vibrational peak at 3363 cm^{-1} confirms the interaction of the O–H groups between XG/PVP/EG. The prominent peaks of XG/PVP/EG at 2942 cm^{-1} and 2870 cm^{-1} are observed in all the blend electrolytes which are attributed to C–H stretching. The significant evidences of cross-linker EG in the solid electrolyte are observed by analyzing the 2000–800 cm^{-1} spectral region. The major changes in the FTIR spectrum are highlighted and shown in Fig. 3b. The peak corresponding to the C = O stretching and C–O bending mode of molecules is observed at 1645 cm^{-1} [27, 43]. The peak at 1645 cm^{-1} reflects the interaction between the XG and PVP [44]. The ester group linkages are formed during the interaction of XG with EG at 1435 cm^{-1}, indicating the symmetrical C = O stretching vibration [36, 45]. The peak at 1286 cm^{-1} is attributed to C–N stretching vibrations. The anhydro glucose ring is identified by peaks in the range of 1026–1056 cm^{-1}, which is a part of the molecular structure in XG [28]. There is a significant decrease in the intensity of the peak at 1039 cm^{-1} which is due to C–O stretching on the polysaccharide skeleton [46] for sample 2 XG/98 PVP. The intensity variations at 1039 cm^{-1} show the interaction between carbonyl groups and the complex nature of the blend electrolyte.

AC impedance analysis

Cole–Cole plot

The ionic conductivity of the blended electrolyte is calculated using AC impedance spectroscopy. Figure 4 shows the Nyquist plot of the blended polymer electrolytes. A semicircle can be seen in the Cole–Cole plot because of both mobile and immobile ions [38]. A semicircle with a spike is observed for all the prepared samples. The Z-view software is used for fitting the semicircle by the construction of an equivalent electrical circuit [47]. In an equivalent circuit, the parallel combination of bulk resistance (R_b) and Constant Phase Element-1 (CPE 1) denotes the
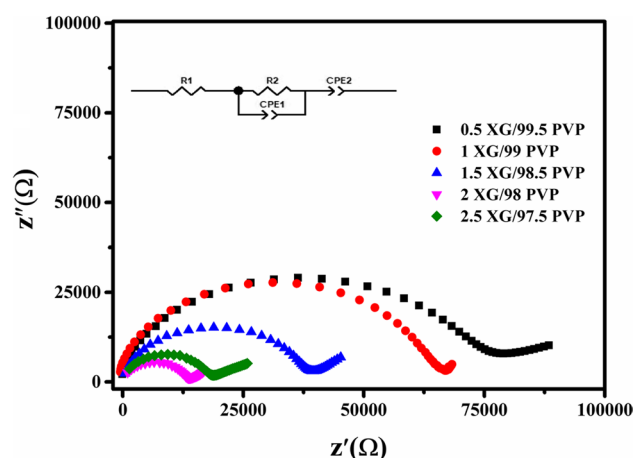

Fig. 4 Cole–Cole plot of Xanthan gum and PVP blend polymer electrolyte

Fig. 3 a FTIR spectrum of 0.5 XG/ 99.5 PVP, 1 XG/99 PVP, 1.5 XG/98.5 PVP, 2 XG/98 PVP, and 2.5 XG/97.5 PVP. **b** FTIR spectrum of 0.5 XG/ 99.5 PVP, 1 XG/99 PVP, 1.5 XG/98.5 PVP, 2 XG/98 PVP, and 2.5 XG/97.5 PVP in the range 2000–800 cm.$^{-1}$

Table 3 Conductivity and activation energy values of XG/PVP blend electrolytes

Samples	Bulk resistance (Ohm)	Constant phase element		Conductivity (S/cm)	Activation energy (eV)
		CPE-1	CPE-2		
0.5 XG/99.5 PVP	76220	5.9×10^{-10}	5.7×10^{-6}	1.18×10^{-7}	0.35
1 XG/99 PVP	66801	2.5×10^{-10}	1.4×10^{-5}	1.69×10^{-7}	0.32
1.5 XG/98.5 PVP	37250	5.5×10^{-10}	7.7×10^{-6}	3.03×10^{-7}	0.29
2 XG/98 PVP	11861	3.1×10^{-10}	3.0×10^{-5}	1.01×10^{-6}	0.21
2.5 XG/97.5 PVP	16610	1.7×10^{-10}	1.4×10^{-6}	7.26×10^{-7}	0.27
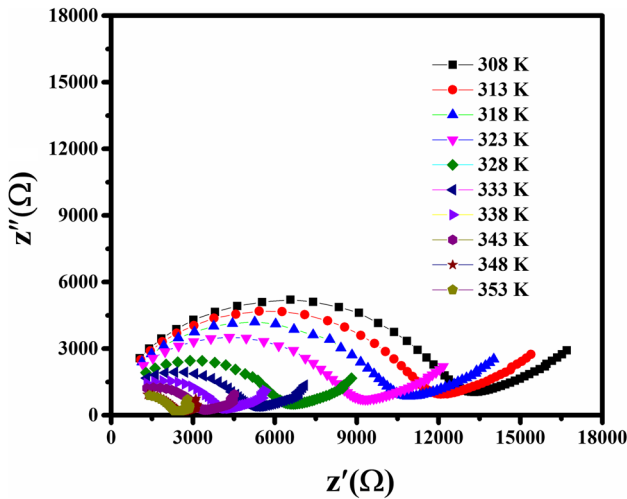
Fig. 5 Cole–Cole plot of 2 XG/98 PVP electrolyte at different temperatures

Fig. 6 Conductance spectra of XG/PVP blend electrolytes

semicircle and series connection of Constant Phase Element-2 (CPE 2) represents the spike at a lower frequency [48]. The conductivity (σ) of polymer electrolyte is calculated by the following equation,

$$\sigma = {}^{t}/_{AR_b} \qquad (1)$$

Here, t is the thickness of the sample, A is the area of the electrode/electrolyte interface, and R_b represents the bulk resistance [49, 50]. The conductivity of pure PVP is reported by SK. Shahenoor Basha et al., as 2.32×10^{-9} S/cm [51]. With the addition of XG, there exists an improvement in the conductivity and the R_b value gets decreased. Compared to the other blends, the 2 XG/98 PVP sample has a low R_b value and higher conductivity of 1.01×10^{-6} S/cm. Further addition of XG with PVP, 2.5 XG/97.5 PVP has an increasing R_b value. These values are listed in Table 3. While increasing the temperature of the sample, the conductivity is also increased owing to the reduction in viscosity. Consequently, the free volume is produced around the polymer chain which causes an increase in the movement of ions [52]. The increase in conductivity with temperature in all polymer electrolytes is shown in Fig. 5.
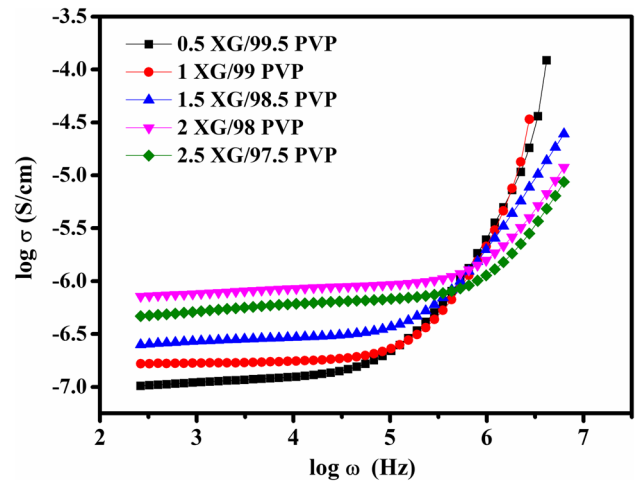
Conductance spectra

The conductance spectra are plotted between the logarithmic frequency (log ω), and its conductivity (log σ) as shown in Fig. 6. The conductance spectra show two regions, namely the plateau region as the low-frequency region (frequency-independent region) and the high-frequency region as a dispersion region [53]. The high-frequency dispersion region is caused by the bulk relaxation phenomenon [54]. Low-frequency region is occurred due to the space-charge polarization at the electrode–electrolyte interface [55]. At high-frequency regions, the conductivity of the polymer electrolytes is increased because of the high oscillatory movement of ions [56]. Figure 7 depicts the temperature-dependent conductance spectra of higher conducting sample 2 XG/98 PVP. A wide plateau region has been observed by increasing the concentration of XG and increasing the temperature of the higher conductivity polymer electrolyte. As described by the free volume theory, the mobility of ions and thereby free volume of the polymer matrix is increased while increasing the temperature.
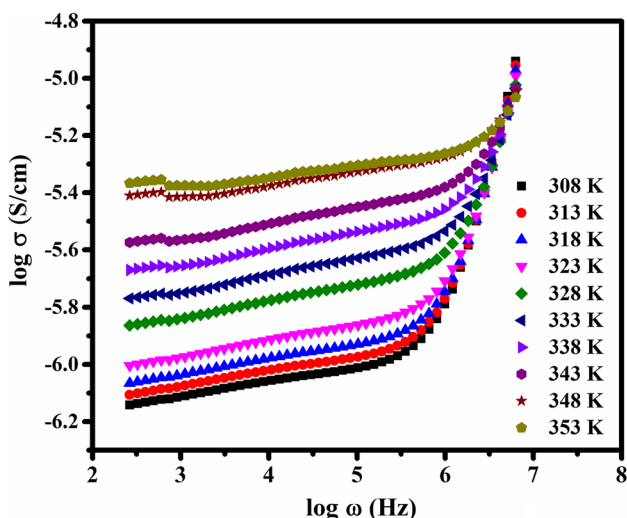
Fig. 7 Conductance spectra of 2 XG/98 PVP sample at different temperatures

Temperature-dependent conductivity

The thermally activated Arrhenius behavior is observed in Fig. 8 which is plotted between 1000/T and log(σ). By increasing the temperature, the conductivity of the sample is also increased. The activation energy (E_a) can be obtained from the linear fit of the Arrhenius plot. The slope value of the fitted data is used to calculate the activation energy (E_a) by the given formula:

$$\sigma = \sigma_\circ exp\left(^{-E_a}/_{KT}\right) \tag{2}$$

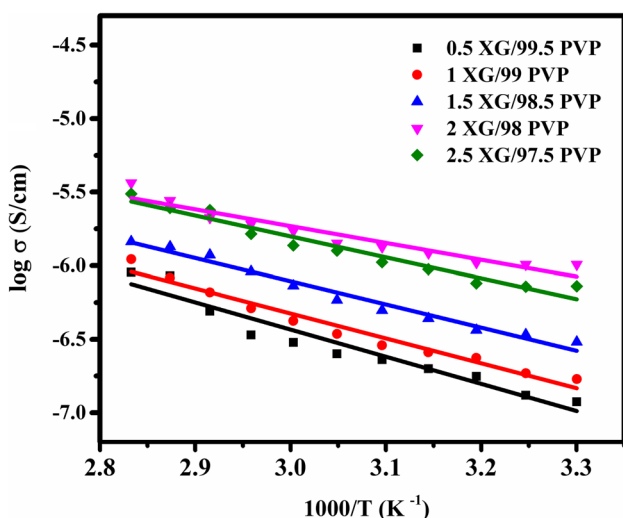In Eq. 2, σ represents conductivity and σ_o is a pre-exponential factor. "K" and "T" denote Boltzmann constant and temperature respectively [57, 58]. The polymeric system 2 XG/98 PVP has a minimum activation energy of 0.21 eV, which is due to the increased segmental mobility within the polymer chain. The variation in the value of activation energy is due to the requirement of energy for the migration of ions. The activation energies (E_a) of the blended electrolytes are calculated and listed in Table 3.

Dielectric spectra analysis

The dielectric properties of prepared electrolytes have investigated in the frequency of 42 Hz to 1 MHz. The real and imaginary parts of complex permittivity (ε') and (ε'') are expressed by the given equations,

$$\varepsilon = \varepsilon' - \varepsilon'' \tag{3}$$

Here, $\varepsilon\prime$, dielectric constant/real part of dielectric permittivity.

ε'', dielectric loss/imaginary part of dielectric permittivity

$$\varepsilon\prime = \left(^{Z''}/_{\omega C_0\left(Z'^2 + Z''^2\right)}\right) \tag{4}$$

$$\varepsilon'' = \left(^{Z'}/_{\omega C_0\left(Z'^2 + Z''^2\right)}\right) \tag{5}$$

Here, ω represents the angular frequency, Z' and Z'' represent the real and imaginary parts of the impedance and C_o denotes the vacuum capacitance [59]. Dielectric constant (ε') and dielectric loss are detected as a function of frequency is shown in Figs. 9 and 10. ε' and ε'' values are significantly diminished as the frequency increases. When the frequency increases, the dielectric values gradually decreases, which may be a result of polarization effects and the inability of
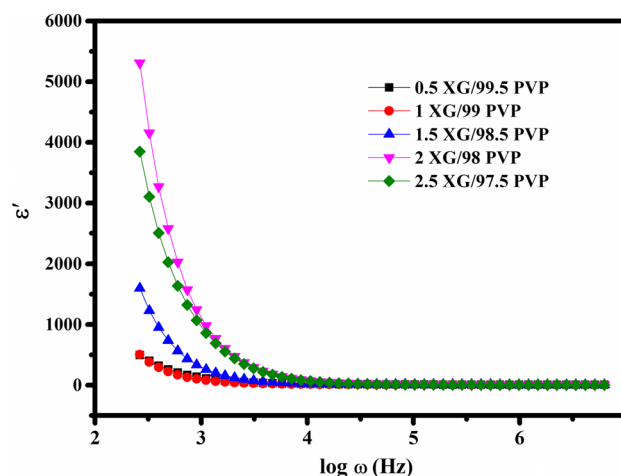

Fig. 8 Arrhenius behavior of XG/PVP blend electrolytes

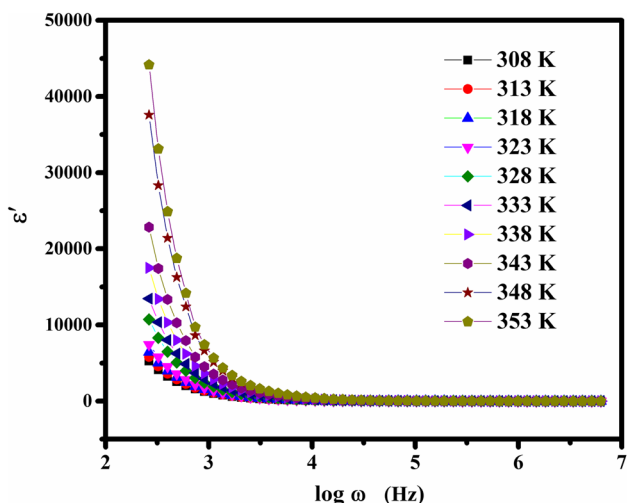**Fig. 9** Logarithmic frequency vs dielectric constant analysis of XG/PVP electrolytes

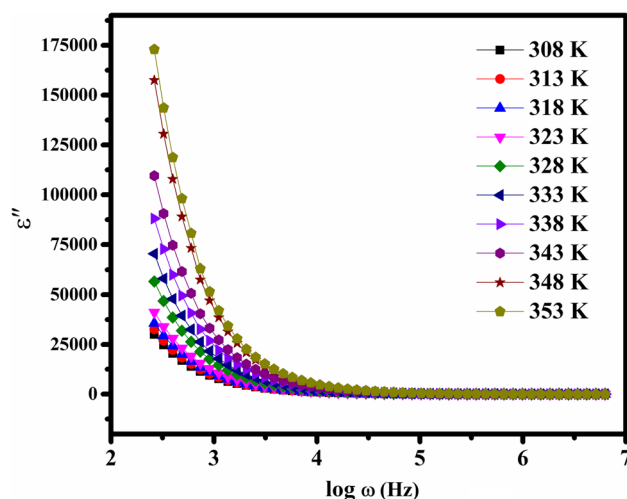**Fig. 10** Logarithmic frequency vs dielectric constant analysis of 2 XG/98 PVP sample at different temperatures

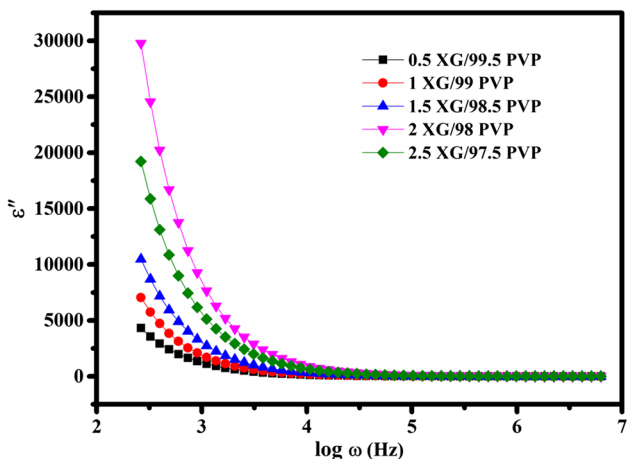**Fig. 12** Logarithmic frequency vs dielectric loss analysis of 2 XG/98 PVP sample at different temperatures

Fig. 11 Logarithmic frequency vs dielectric loss analysis of XG/PVP electrolytes
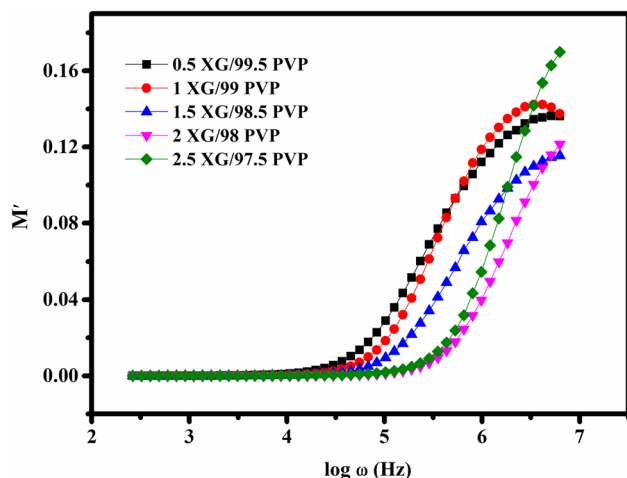

Fig. 13 Logarithmic frequency vs real part of dielectric modulus analysis of XG/PVP electrolytes

the dipoles to detect the field variation at higher frequencies [60]. The real part of the dielectric permittivity is used for the observation of dipole orientation or polarization. The imaginary part refers to the dielectric loss which indicates the energy required to align the dipoles [61]. At high frequencies, the dielectric constant decreases because the applied electric field is lower than the dipole rotation [62]. Polarization occurring at the electrode/electrolyte interfaces and the dipolar relaxation process is responsible for the decrease in the dielectric constant with increasing frequency [63]. Minimal polarization of the dielectric material results from the sudden inversion of the electric field which occurs at a higher frequency and prevents the diffusion of ions along its path [64].

Figures 11 and 12 show the variation of temperature with the real and imaginary parts of the dielectric permittivity. It is noticed that the value of $\varepsilon\prime$ and ε'' significantly increase at higher temperatures in the lower frequency range due to electrode polarization and decrease at higher frequencies, which is evidence of fast periodic reversal of the electric field.

Modulus spectra

The real and imaginary parts of the dielectric moduli (M' and M'') are shown in Figs. 13 and 14, respectively. Modulus spectra are plotted between logarithmic frequency and dielectric modulus and the formulae are given below,
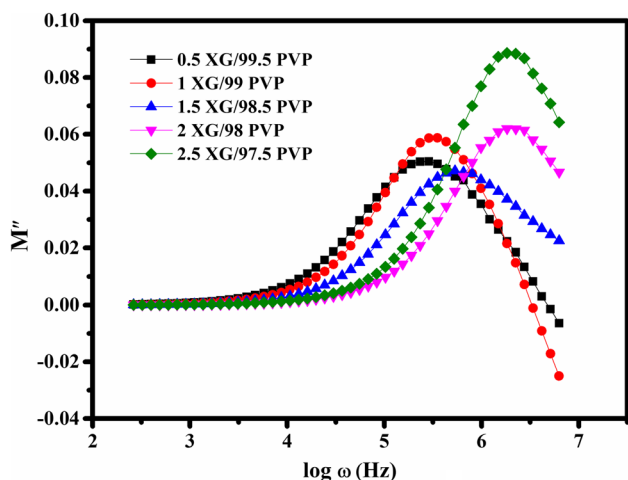
Fig. 14 Logarithmic frequency vs Imaginary part of dielectric modulus analysis of XG/PVP electrolytes

$$M' = \left(\frac{\varepsilon'}{[\varepsilon'^2 + \varepsilon''^2]} \right) \qquad (6)$$

$$M'' = \left(\frac{\varepsilon''}{[\varepsilon'^2 + \varepsilon''^2]} \right) \qquad (7)$$

In Eqs. 6 and 7, M' and M'' represent real and imaginary parts of the dielectric modulus values [50]. The long tail is observed at nearly zero at low frequencies. The peak in the modulus spectra is shifted from the low-frequency to the high-frequency region while increasing the concentration of XG. This is due to the large capacitance associated with electrodes, which encourages the migration of ions for conduction [49, 65]. The bulk effect causes the modulus values to increase gradually as the frequency increases. This proves that the blended electrolytes exhibit non-Debye behavior [48]. Electrode polarization is observed without any dispersion, and an extended tail is noted at a low frequency, which reveals the capacitive behavior of the electrolytes [66]. At higher frequencies, a maximum shift is observed for the higher-conducting sample 2 XG/98 PVP.

Argand plot

For the confirmation of the non-Debye nature of the polymer electrolytes, an Argand plot is plotted between the real and imaginary parts of the modulus for all XG/PVP blend electrolytes as shown in Fig. 15. A smaller semicircle arc radius represents a shorter ion relaxation time in polymer electrolytes. In the Argand plot, a sample with higher conductivity has a small semicircle arc and a shorter relaxation time [40]. Various types of polarization and relaxation mechanisms, as well as different interactions between ions and dipoles, contribute to the non-Debye nature. The conductivity of a
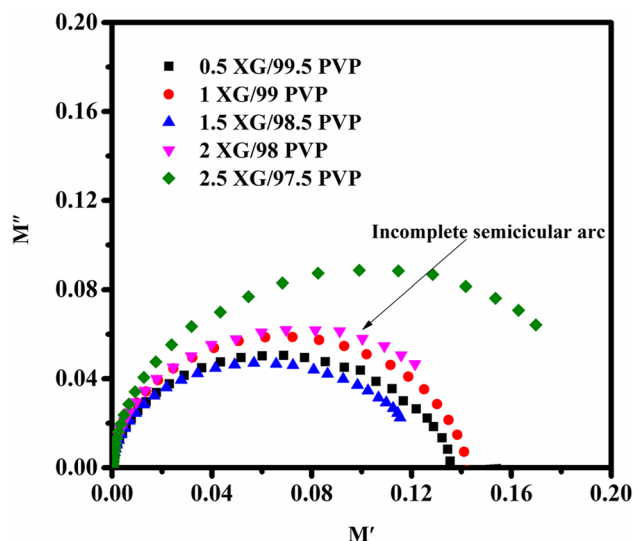
polymer electrolyte is closely related to the arc radius [67]. The higher-conducting sample 2 XG/ 98 PVP shows a short incomplete semicircle arc. It has recently been demonstrated that conductivity relaxation, in which polymer chain motion assists ions migration, and no coupling between polymer/ cation motion occurs. This may be responsible for the Argand plot with a perfect semi-circular arc linked to the relaxation process [68]. In Fig. 16, the incomplete semi-circles in the argand plot curves at different temperatures clearly show non-Debye behavior.
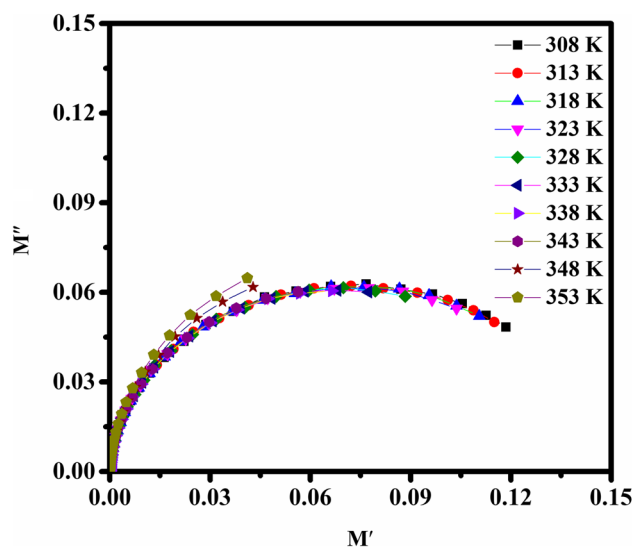

Fig. 15 Complex modulus spectrum of XG/PVP blend samples

Fig. 16 Complex modulus spectrum of higher conducting sample at different temperatures

Dissipation factor (tanδ)

The dielectric loss factor (tanδ) is a frequency-dependent variable used for analyzing the electrical characteristics of polymers and represents the energy dissipation factor in the dielectric. A tangent spectrum is drawn between the logarithmic frequency and tanδ for all prepared electrolytes as shown in Fig. 17. The interfacial polarization effect may be responsible for the broad dispersion peak observed at low frequencies, and dipolar relaxation may be responsible for the dispersion observed at higher frequencies. Shifting of the peaks toward a higher frequency represents the existence of more ions for conduction, which minimizes the sample resistivity [69]. The loss tangent can be expressed as,

$$\tan\delta = \varepsilon'/\varepsilon'', \qquad (8)$$

Here, ε' and ε'' denote the real and imaginary parts of dielectric parameters [70]. The variation in the tangent loss with log frequency for different temperatures is shown in Fig. 18. The relaxation time (τ) is calculated from tan δ spectra, and can be described by Kohlrausch–Williams–Watts law.

$$\omega\tau = 1 \qquad (9)$$

$$\varphi(t) = exp^{\left(\frac{-t}{\tau}\right)^{\beta}} \qquad (10)$$

$$\beta = 1.14/FWHM \qquad (11)$$

ω represents the angular frequency, β represents Kohlrausch exponent, and FWHM denotes full width half maximum [49]. The relaxation time (τ) of the higher conducting sample (2 XG/98 PVP) is minimum as 6.20×10^{-5} s. As per the
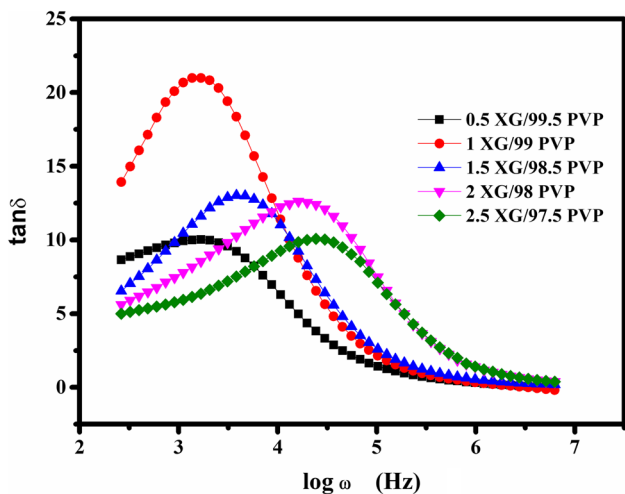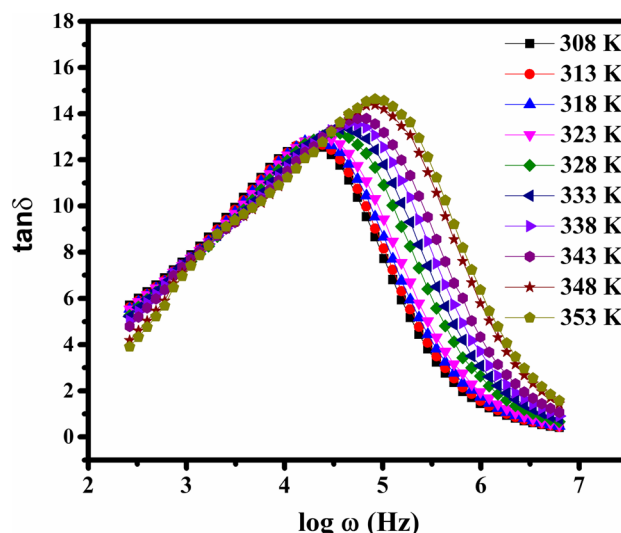

Fig. 18 Tangent spectra of 2 XG/98 PVP sample at different temperatures

non-Debye model, the value of β is less than unity ($0 < \beta < 1$) [40, 71] for all the samples. The calculated values are given in Table 4.

Transference number analysis

For all compositions of polymer electrolyte systems, the transference number corresponding to ionic (t_{ion}) and electronic (t_{ele}) transport are determined and shown in Fig. 19. One of the fundamental techniques used for determining the transference number is Wagner's DC polarization method [72]. The prepared polymer electrolyte is sandwiched between the two-silver electrodes and fixed DC voltage of 2 V is applied. One silver electrode is coated with a graphite that acts as an electronic transport barrier. In this method, direct current (DC) is monitored by the function of time [73]. The current value is decreased with time. The polarization current decreases rapidly over time if ions are the major charge carriers, but it will not diminish over time if electrons are dominant [74]. The transference number of the blend electrolytes is calculated by the given equation,

Fig. 17 Tangent spectra of XG/PVP electrolytes

Table 4 Relaxation time and Kohlrausch exponent parameter

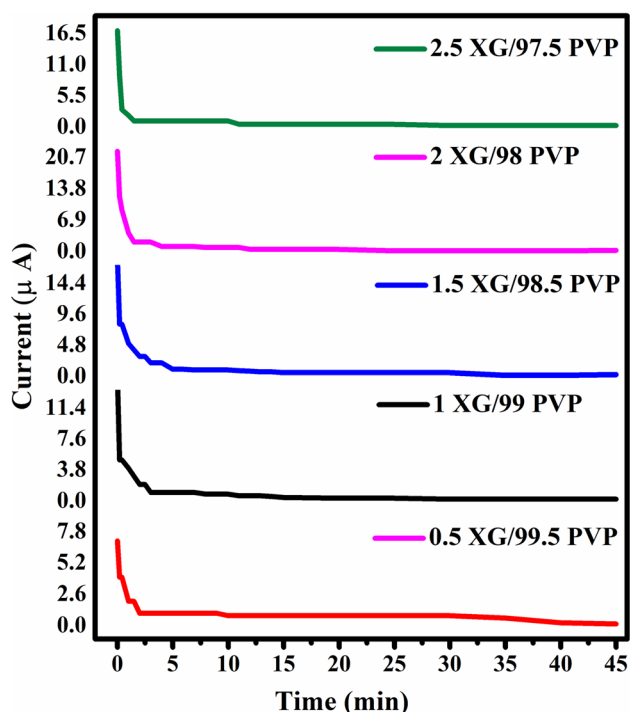| Samples	Relaxation time τ (s)	FWHM	β
0.5 XG/99.5 PVP	5.9×10^{-4}	1.78	0.63
1 XG/99 PVP	7.3×10^{-4}	1.67	0.68
1.5 XG/98.5 PVP	2.6×10^{-4}	2.02	0.56
2 XG/98 PVP	6.2×10^{-5}	2.41	0.47
2.5 XG/97.5 PVP	4.1×10^{-5}	2.65	0.43

Fig. 19 Transference number analysis of XG/PVP blend electrolytes

Table 5 Transference number analysis

Sample	t_{ion}	t_{ele}
0.5 XG/99.5 PVP	0.9857	0.01428
1 XG/99 PVP	0.9866	0.01333
1.5 XG/98.5 PVP	0.9888	0.01111
2 XG/98 PVP	0.9909	0.00909
2.5 XG/97.5 PVP	0.9882	0.01176

$$t_{ion} = \left(I_i - I_f / I_i \right) \tag{12}$$

$$t_{ele} = \left(I_f / I_i \right) \tag{13}$$

Here, t_{ion} represents the transport number of ions, t_{ele} denotes the transport number of electrons, I_i is the initial current, and I_f represents the final current [50]. The transference number of both ions (t_{ion}) and electrons (t_{ele}) are tabulated for all the blends (Table 5). The value of t_{ion} for all the blend electrolytes are above 0.98 and it is confirmed that the charge transport of the blend electrolytes is due to hydrogen ions. The transference number value is close to unity and confirms the domination of hydrogen ions in a polymer electrolyte [75].

Conclusion

A blend polymer electrolyte using XG and PVP with 0.65 ml of EG as a cross-linker is synthesized by the solution casting method. The amorphous nature of XG is increased by blending with PVP, as confirmed by XRD analysis. The FTIR observations demonstrate that the interaction of XG and PVP is due to a slight change in the wavenumber at 1645 cm^{-1} due to pyrrolidone rings and the stretching modes of the carbonyl bonds. The blending of XG with EG at 1435 cm^{-1} indicates the symmetrical C–O stretching vibration. The maximum conductivity is calculated as 1.01×10^{-6} S/cm for sample 2 XG/98 PVP using AC impedance analysis at room temperature. Arrhenius behavior is observed for all the blends and minimum activation Energy (E_a) 0.14 eV is calculated for the sample 2 XG/98 PVP from the temperature-dependent plot. The dielectric properties of the frequency- and temperature-dependent spectra are plotted and their characteristics were studied. The non-Debye nature of the blend polymer system is proved by the dielectric modulus spectra, Argand plot, and tangent spectra. From the tangent spectra analysis, the lowest relaxation time (τ) is denoted as 6.2×10^{-5} s, for the higher conducting sample. The non-Debye nature of the polymer electrolytes is confirmed by the β ($0 < \beta < 1$), value observed from the tangent spectra. TNA analysis is taken for the confirmation of the conductivity due to protons in all blend electrolytes.

Data availability The datasets used and/or analyzed during the current study are available from the corresponding author upon reasonable request.

Declarations

Competing interests The authors declare no competing interests.

Ethical approval Not applicable.

Conflict of interest The authors declare no competing interests.

References

1. Raphael E, Avellaneda CO, Manzolli B, Pawlicka A (2010) Agar-based films for application as polymer electrolytes. Electrochim Acta 55:1455–1459. https://doi.org/10.1016/j.electacta.2009.06.010

2. Chen F, Yang D, Zha W et al (2017) Solid polymer electrolytes incorporating cubic Li7La3Zr2O12 for all-solid-state lithium rechargeable batteries. Electrochim Acta 258:1106–1114. https://doi.org/10.1016/j.electacta.2017.11.164

3. Chua S, Fang R, Sun Z et al (2018) Hybrid solid polymer electrolytes with two-dimensional inorganic nanofillers. Chem - A Eur J 24:18180–18203. https://doi.org/10.1002/chem.201804781

4. Hamad K, Kaseem M, Ko YG, Deri F (2014) Biodegradable polymer blends and composites: an overview. Polym Sci - Ser A 56:812–829

5. Hir ZAM, Daud S, Rafaie HA, et al (2021) Polymer-based flexible substrates for flexible supercapacitors. Flex Supercapacitor Nanoarchitectonics 59–93. https://doi.org/10.1002/9781119711469.ch4

6. Taifan W, Boily JF, Baltrusaitis J (2016) Surface chemistry of carbon dioxide revisited. Surf Sci Rep 71:595–671. https://doi.org/10.1016/j.surfrep.2016.09.001

7. Muthuraj R, Misra M, Mohanty AK (2018) Biodegradable compatibilized polymer blends for packaging applications: a literature review. J Appl Polym Sci 135

8. Priya SS, Karthika M, Selvasekarapandian S, et al (2018) Study of biopolymer I-carrageenan with magnesium perchlorate

9. Khanmirzaei MH, Ramesh S (2013) Ionic transport and FTIR properties of lithium iodide doped biodegradable rice starch based polymer electrolytes. 8:9977–9991

10. Sahalianov I, Say MG, Abdullaeva OS et al (2021) Volumetric double-layer charge storage in composites based on conducting polymer PEDOT and cellulose. ACS Appl Energy Mater 4:8629–8640. https://doi.org/10.1021/acsaem.1c01850

11. Koh JCH, Ahmad ZA, Mohamad AA (2012) Bacto agar-based gel polymer electrolyte. Ionics (Kiel) 18:359–364. https://doi.org/10.1007/s11581-011-0631-6

12. Selvalakshmi S, Vanitha D, Saranya P et al (2022) Structural and conductivity studies of ammonium chloride doped agar–agar biopolymer electrolytes for electrochemical devices. J Mater Sci Mater Electron 33:24884–24894. https://doi.org/10.1007/s10854-022-09198-2

13. Vijaya N, Selvasekarapandian S, Sornalatha M et al (2017) Proton-conducting biopolymer electrolytes based on pectin doped with NH4X (X=Cl, Br). Ionics (Kiel) 23:2799–2808. https://doi.org/10.1007/s11581-016-1852-5

14. Rajeswari A, Stobel Christy EJ, Pius A (2021) Biopolymer blends and composites. In: Biopolymers and their Industrial Applications. Elsevier, pp 105–147

15. Che Balian SR, Ahmad A, Mohamed NS (2016) The effect of lithium iodide to the properties of carboxymethyl κ-carrageenan/carboxymethyl cellulose polymer electrolyte and dye-sensitized solar cell performance. Polymers (Basel) 8. https://doi.org/10.3390/polym8050163

16. Hadi JM, Aziz SB, Kadir MFZ, et al (2021) Design of plasticized proton conducting Chitosan:Dextran based biopolymer blend electrolytes for EDLC application: Structural, impedance and electrochemical studies. Arab J Chem 14. https://doi.org/10.1016/j.arabjc.2021.103394

17. Jenova I, Venkatesh K, Karthikeyan S et al (2021) Characterization of solid polymer electrolyte based on gum tragacanth and lithium nitrate. Polym Technol Mater 00:1–15. https://doi.org/10.1080/25740881.2021.1934018

18. Aziz SB, Asnawi ASFM, Mohammed PA et al (2021) Impedance, circuit simulation, transport properties and energy storage behavior of plasticized lithium ion conducting chitosan based polymer electrolytes. Polym Test 101:107286. https://doi.org/10.1016/j.polymertesting.2021.107286

19. Aziz SB, Abdulwahid RT, Kadir MFZ et al (2022) Design of non-faradaic EDLC from plasticized MC based polymer electrolyte with an energy density close to lead-acid batteries. J Ind Eng Chem 105:414–426

20. Abdulwahid RT, Aziz SB, Kadir MFZ (2022) Insights into ion transport in biodegradable solid polymer blend electrolyte based on FTIR analysis and circuit design. J Phys Chem Solids 167:110774

21. Hadi JM, Aziz SB, Ghafur Rauf H et al (2022) Proton conducting polymer blend electrolytes based on MC: FTIR, ion transport and electrochemical studies. Arab J Chem 15:104172. https://doi.org/10.1016/j.arabjc.2022.104172

22. Abdulwahid RTB, Aziz S, Kadir MFZ (2022) Design of proton conducting solid biopolymer blend electrolytes based on chitosan-potato starch biopolymers: deep approaches to structural and ion relaxation dynamics of H+ ion. J Appl Polym Sci 139:e52892

23. Aziz SB, Hamsan MH, Nofal MM, et al (2020) Structural, impedance and electrochemical characteristics of electrical double layer capacitor devices based on Chitosan: Dextran biopolymer blend electrolytes. Polymers (Basel) 12. https://doi.org/10.3390/polym12061411

24. Rauf H, Hadi JM, Abdulwahid RT, Mustafa MS (2022) A novel approach to design high resistive polymer electrolytes based on a novel approach to design high resistive polymer electrolytes based on PVC : electrochemical impedance and dielectric properties. https://doi.org/10.20964/2022.05.04

25. Becker A, Katzen F, Pühler A, Ielpi L (1998) Xanthan gum biosynthesis and application: a biochemical/genetic perspective. Appl Microbiol Biotechnol 50:145–152. https://doi.org/10.1007/s002530051269

26. Abu Elella MH, Hanna DH, Mohamed RR, Sabaa MW (2022) Synthesis of xanthan gum/trimethyl chitosan interpolyelectrolyte complex as pH-sensitive protein carrier. Polym Bull 79:2501–2522. https://doi.org/10.1007/s00289-021-03656-3

27. Sharma V, Kumar R, Arora N et al (2020) Effect of heat treatment on thermal and mechanical stability of NaOH-doped xanthan gum-based hydrogels. J Solid State Electrochem 24:1337–1347. https://doi.org/10.1007/s10008-020-04641-y

28. Sudhakar YN, Selvakumar M, Krishna Bhat D (2015) Lithium salts doped biodegradable gel polymer electrolytes for supercapacitor application. J Mater Environ Sci 6:1218–1227

29. Zhang S, Yu N, Zeng S et al (2018) An adaptive and stable bio-electrolyte for rechargeable Zn-ion batteries. J Mater Chem A 6:12237–12243. https://doi.org/10.1039/c8ta04298e

30. Kumar A, Rao KM, Han SS (2017) Application of xanthan gum as polysaccharide in tissue engineering : a review. Carbohydr Polym. https://doi.org/10.1016/j.carbpol.2017.10.009

31. Polu AR, Kumar R, Rhee HW (2015) Magnesium ion conducting solid polymer blend electrolyte based on biodegradable polymers and application in solid-state batteries. Ionics (Kiel) 21:125–132. https://doi.org/10.1007/s11581-014-1174-4

32. Shahenoor Basha SK, Gnanakiran M, Ranjit Kumar B et al (2017) Synthesis and spectral characterization on PVA/PVP: Go based blend polymer electrolytes. Rasayan J Chem 10:1159–1166. https://doi.org/10.7324/rjc.2017.1041756

33. Caldeira I, Lüdtke A, Tavares F et al (2018) Ecologically friendly xanthan gum-PVA matrix for solid polymeric electrolytes. Ionics (Kiel) 24:413–420. https://doi.org/10.1007/s11581-017-2223-6

34. Blends ÁPVPÁ (2010) Miscibility studies of polysaccharide xanthan gum/PVP blend. 135–140. https://doi.org/10.1007/s10924-010-0191-2

35. Sakakibara T, Kitamura M, Honma T et al (2019) Cross-linked polymer electrolyte and its application to lithium polymer battery. Electrochim Acta 296:1018–1026. https://doi.org/10.1016/j.electacta.2018.11.155

36. Cholant CM, Ely F, Santos MJL, et al (2019) Electrochimica Acta Dielectric behavior and FTIR studies of xanthan gum-based solid polymer electrolytes. 305:232–239.https://doi.org/10.1016/j.electacta.2019.03.055

37. Tavares FC, Dörr DS, Pawlicka A, Oropesa Avellaneda C (2018) Microbial origin xanthan gum-based solid polymer electrolytes. J Appl Polym Sci 135:1–6. https://doi.org/10.1002/app.46229

38. Jothi MA, Vanitha D, Bahadur SA, Nallamuthu N (2021) Proton conducting polymer electrolyte based on cornstarch, PVP, and NH4Br for energy storage applications. Ionics (Kiel) 27:225–237. https://doi.org/10.1007/s11581-020-03792-2

39. Călina I, Demeter M, Scărişoreanu A, Micutz M (2021) Development of novel superabsorbent hybrid hydrogels by e-beam crosslinking. Gels 7:1–18. https://doi.org/10.3390/gels7040189

40. Anandha Jothi M, Vanitha D, Nallamuthu N, et al (2020) Investigations of lithium ion conducting polymer blend electrolytes using biodegradable cornstarch and PVP. Phys B Condens Matter 580. https://doi.org/10.1016/j.physb.2019.411940

41. Çabuk H, Yılmaz Y, Yıldız E (2019) A vortex-assisted deep eutectic solvent-based liquid-liquid microextraction for the analysis of alkyl gallates in vegetable oils. Acta Chim Slov 66:385–394. https://doi.org/10.17344/acsi.2018.4877

42. Tran PH, Thi Hang AH (2018) Deep eutectic solvent-catalyzed arylation of benzoxazoles with aromatic aldehydes. RSC Adv 8:11127–11133. https://doi.org/10.1039/c8ra01094c

43. Bands CA, Liu X 6. 3 : IR spectrum and characteristic absorption bands. 1–3

44. Rajeswari N, Selvasekarapandian S, Prabu M et al (2013) Lithium ion conducting solid polymer blend electrolyte based on biodegradable polymers. Bull Mater Sci 36:333–339. https://doi.org/10.1007/s12034-013-0463-2

45. Coates J (2006) Interpretation of infrared spectra, a practical approach. Encycl Anal Chem 10815–10837. https://doi.org/10.1002/9780470027318.a5606

46. Chai MN, Isa MIN (2013) The oleic acid composition effect on the carboxymethyl cellulose based biopolymer electrolyte. J Cryst Process Technol 03:1–4. https://doi.org/10.4236/jcpt.2013.31001

47. Gonçalves R, Pereira EC, Marchesi LF (2017) The overoxidation of poly(3-hexylthiophene) (P3HT) thin film: CV and EIS measurements. Int J Electrochem Sci 12:1983–1991. https://doi.org/10.20964/2017.03.44

48. Nandhinilakshmi M, Vanitha D, Nallamuthu N et al (2022) Structural, electrical behavior of sodium ion-conducting corn starch–PVP-based solid polymer electrolytes. Polym Bull. https://doi.org/10.1007/s00289-022-04230-1

49. Nandhinilakshmi M, Vanitha D, Nallamuthu N et al (2022) Investigation on conductivity and optical properties for blend electrolytes based on iota-carrageenan and acacia gum with ethylene glycol. J Mater Sci Mater Electron 33:21172–21188. https://doi.org/10.1007/s10854-022-08925-z

50. Nandhinilakshmi M, Vanitha D, Nallamuthu N et al (2022) Dielectric relaxation behaviour and ionic conductivity for corn starch and PVP with sodium fluoride. J Mater Sci Mater Electron 33:12648–12662. https://doi.org/10.1007/s10854-022-08214-9

51. Shahenoor Basha S, Sunita Sundari G, Vijay Kumar K et al (2017) Electrical conduction behaviour of PVP based composite polymer electrolytes. Rasayan J Chem 10:279–285. https://doi.org/10.7324/RJC.2017.1011612

52. Farhana NK, Omar FS, Shanti R et al (2019) Iota-carrageenan-based polymer electrolyte: impact on ionic conductivity with incorporation of AmNTFSI ionic liquid for supercapacitor. Ionics (Kiel) 25:3321–3329. https://doi.org/10.1007/s11581-019-02865-1

53. Muthuvinayagam M, Sundaramahalingam K (2021) Characterization of proton conducting poly[ethylene oxide]: poly[vinyl pyrrolidone] based polymer blend electrolytes for electrochemical devices. High Perform Polym 33:205–216. https://doi.org/10.1177/0954008320953467

54. Jenova I, Venkatesh K, Madeswaran KS et al (2021) Solid polymer electrolyte based on tragacanth gum - ammonium thiocyanate. J Solid State Electrochem. https://doi.org/10.1007/s10008-021-05016-7

55. Karpagavel S, Sundaramahalingam K, Vanitha AMD, Nagarajan AMER (2021) Electrical properties of lithium - ion conducting poly (vinylidene fluoride - co - hexafluoropropylene) (PVDF - HFP)/polyvinylpyrrolidone (PVP) solid polymer electrolyte. J Electron Mater. https://doi.org/10.1007/s11664-021-08967-9

56. Sundaramahalingam K, Karpagavel K, Jayanthi S, et al (2021) Structural and electrical behaviours of amino acid-based solid polymer electrolytes. Bull Mater Sci 44. https://doi.org/10.1007/s12034-021-02464-9

57. Jothi MA, Vanitha D, Bahadur SA, Nallamuthu N (2021) Promising biodegradable polymer blend electrolytes based on cornstarch : PVP for electrochemical cell applications. Bull Mater Sci 0123456789:1–12. https://doi.org/10.1007/s12034-021-02350-4

58. Sundaramahalingam K, Jayanthi S, Vanitha D, Nallamuthu N (2021) Dielectric studies of designed novel sodium-based polymer electrolyte with the effect of adding amino acid. Ionics (Kiel) 27:3919–3932. https://doi.org/10.1007/s11581-021-04116-8

59. Jothi MA, Vanitha D (2021) Investigations of biodegradable polymer blend electrolytes based on Cornstarch : PVP : NH4Cl and its potential application in solid-state batteries. J Mater Sci Mater Electron 32:5427–5441. https://doi.org/10.1007/s10854-021-05266-1

60. Irfan M, Manjunath A, Mahesh SS et al (2021) Influence of NaF salt doping on electrical and optical properties of PVA/PVP polymer blend electrolyte films for battery application. J Mater Sci Mater Electron 32:5520–5537. https://doi.org/10.1007/s10854-021-05274-1

61. Aziz SB, Brza MA, Mohamed PA et al (2019) Increase of metallic silver nanoparticles in Chitosan:AgNt based polymer electrolytes incorporated with alumina filler. Results Phys 13:102326. https://doi.org/10.1016/j.rinp.2019.102326

62. Arasakumari M (2021) Effect of anhydrous Gdcl3 doping on the structural, optical and electrical properties of PVP polymer electrolyte films

63. Basha SKS, Sundari GS, Kumar KV (2016) Structural and dielectric properties of PVP based composite polymer electrolyte thin films. J Inorg Organomet Polym Mater. https://doi.org/10.1007/s10904-016-0487-3

64. Teo LP, Buraidah MH, Nor AFM, Majid SR (2012) Conductivity and dielectric studies of Li 2SnO 3. Ionics (Kiel) 18:655–665. https://doi.org/10.1007/s11581-012-0667-2

65. Brza MA, Aziz SB, Nofal MM, et al (2020) Drawbacks of low lattice energy ammonium salts for ion-conducting polymer electrolyte preparation: structural, morphological and electrical characteristics of CS:PEO:NH4BF4-based polymer blend electrolytes. Polymers (Basel) 12. https://doi.org/10.3390/POLYM12091885

66. Transport BI, Alshehri SM, Ahamad T, Kadir MFZ (2021) The study of plasticized sodium ion conducting polymer blend electrolyte membranes based on chitosan/dextran potential stability. 1–24

67. Sundaramahalingam K, Vanitha D, Nallamuthu N et al (2018) Electrical properties of lithium bromide poly ethylene oxide / poly vinyl pyrrolidone polymer blend elctrolyte. Phys B Phys Condens Matter. https://doi.org/10.1016/j.physb.2018.10.040

68. Ahmed MB, Nofal MM, Aziz SB et al (2022) The study of ion transport parameters associated with dissociated cation using EIS model in solid polymer electrolytes (SPEs) based on PVA host polymer: XRD, FTIR, and dielectric properties. Arab J Chem 15:104196. https://doi.org/10.1016/j.arabjc.2022.104196

69. Rajeswari N, Selvasekarapandian S, Sanjeeviraja C et al (2014) A study on polymer blend electrolyte based on PVA/PVP with proton salt. Polym Bull 71:1061–1080. https://doi.org/10.1007/s00289-014-1111-8

70. Mohamad AH, Abdullah OG, Saeed SR (2020) Effect of very fine nanoparticle and temperature on the electric and dielectric properties of MC-PbS polymer nanocomposite films. Results Phys 16. https://doi.org/10.1016/j.rinp.2019.102898

71. Dutta P, Biswas S, De Kumar S (2002) Dielectric relaxation in polyaniline-polyvinyl alcohol composites. Mater Res Bull 37:193–200. https://doi.org/10.1016/S0025-5408(01)00813-3

72. Agrawal RC, Hashmi SA, Pandey GP (2007) Electrochemical cell performance studies on all-solid-state battery using nano-composite polymer electrolyte membrane. Ionics (Kiel) 13:295–298. https://doi.org/10.1007/s11581-007-0112-0

73. Hema M, Selvasekerapandian S, Sakunthala A et al (2008) Structural, vibrational and electrical characterization of PVA-NH4Br polymer electrolyte system. Phys B Condens Matter 403:2740–2747. https://doi.org/10.1016/j.physb.2008.02.001

74. Shukur MF, Ithnin R, Kadir MFZ (2016) Ionic conductivity and dielectric properties of potato starch-magnesium acetate biopolymer electrolytes: the effect of glycerol and 1-butyl-3-methylimidazolium chloride. Ionics (Kiel) 22:1113–1123. https://doi.org/10.1007/s11581-015-1627-4

75. Hadi JM, Aziz SB, Mustafa MS et al (2020) Role of nano-capacitor on dielectric constant enhancement in PEO:NH4SCN:xCeO2 polymer nano-composites: electrical and electrochemical properties. J Mater Res Technol 9:9283–9294. https://doi.org/10.1016/j.jmrt.2020.06.022